Quantitative Measurements of Enhanced Soot Production in a Flickering Methane/Air Diffusion Flame

CHRISTOPHER R. SHADDIX,[†] JOEL E. HARRINGTON,*[†] and KERMIT C. SMYTH[‡]

Building and Fire Research Laboratory, National Institute of Standards and Technology, Gaithersburg, MD 20899

Integrated models of soot production and oxidation are based upon experimental results obtained in steady, laminar flames. For successful application of these descriptions to turbulent combustion, it is instructive to test predictions of soot concentrations against experimental measurements obtained in time-varying flowfields. This paper reports quantitative measurements of the local soot volume fraction in a co-flowing, flickering CH_4/air diffusion flame burning at atmospheric pressure. Acoustic forcing of the fuel flow rate is used to phase lock the periodic flame flicker close to the natural flicker frequency. Our measurements show that soot production is four times greater for a forcing condition in which flame tip clipping occurs, compared with a steady flame burning with the same mean fuel flow velocity. The soot field in the flickering flame has been characterized using tomographic reconstruction of extinction data obtained at 632.8 nm, laser-induced incandescence (LII) images calibrated against steady CH_4/air extinction results, and vertically polarized scattering data. The LII method is found to track the soot volume fraction closely and to give better signal-to-noise than the extinction measurements in both the steady and time-varying flowfields. A Mie analysis of these results suggests that the flickering flame exhibits similar number densities but larger particle sizes than the corresponding steady flame.

INTRODUCTION

As our understanding of gas-phase chemistry in steady diffusion flames has matured, increased focus has been directed toward more practical, turbulent diffusion flames. A critical assumption in applying chemical models developed in laminar flames to turbulent combustion is that the limited combinations of residence times, temperature histories, local stoichiometries (mixture fraction), and strain rates (scalar dissipation) sampled in laboratory-scale steady laminar flames are sufficient to quantitatively describe chemical processes in turbulent environments. In order to critically evaluate the validity of this assumption, an experimental facility for performing optical measurements in time-varying, laminar diffusion flames has been developed at NIST [1]. This apparatus provides an environment for in situ investigation of flame chemistry, which allows the systematic examination of the time-dependent interaction of variable-strength external vortex rings with the flame structure.

In the absence of a significant oxidizer coflow, most laboratory diffusion flames flicker naturally at a frequency between 10 and 20 Hz even at fairly modest fuel flow velocities (5–10 cm/s). Indeed, pool fires and transitional jet diffusion flames also exhibit flickering behavior, with a frequency dependence on fuel tube or pool diameter expressed as $f \sim 1.5/(D)^{1/2}$ (for f in hertz and D in meters) [2, 3], largely independent of the fuel flow rate. This flickering results from the cyclical formation and convection of vortex rings external to the flame sheet [4–6]. The large vortical structures apparently form due to a Kelvin-Helmholtz type of hydrodynamic instability which arises from the buoyant acceleration of the high-temperature, low-density gases and the resulting shear with the more slowly moving coflow [5–7]. Previous researchers have found that the flickering tendency of diffusion flames may be locked near the natural flicker frequency by applying a small periodic perturbation to the fuel flow

* Present address: SRI International, Molecular Physics Laboratory, Menlo Park, CA 94025.

† National Research Council NIST Postdoctoral Research Associate.

‡ Corresponding author.

Presented at the Twenty-Fifth Symposium (International) on Combustion, Irvine, California, 31 July–5 August 1994.

Published by Elsevier Science Inc.

0010-2180/94/$7.00

[8–11]. In the present study optical diagnostics are phase-locked to a sinusoidal oscillation of the fuel stream at the ~ 10 Hz repetition rate of a Nd^{3+}:YAG laser, permitting phase-specific measurements to be performed in a time-varying flowfield.

In an earlier study of OH · laser-induced fluorescence and elastic scattering from soot in steady and time-varying methane/air flames [1], it was found that the soot scattering intensity in the time-varying flame was significantly greater than that observed for the steady (i.e., unforced) flame with the same mean fuel and air flow rates. For a particular forcing and phase condition in which flame tip clipping occurred, the horizontally polarized scattering intensity was quantified and showed over a factor of 7 enhancement. The OH · fluorescence and soot scattering fields for this flickering flame and its steady counterpart are shown in Fig. 1, to aid in the interpretation of the experimental results to follow. Previous investigators of flickering flames often have imaged the soot layer using luminosity signals [4, 8, 9, 11], but no quantitative soot measurements or comparisons with steady flame soot signals were reported.

The enhancement in soot formation implied by the increased scattering in flickering flames should provide a demanding test of the ability of recently formulated integrated soot models [12–15] to accurately predict soot formation and oxidation rates in combusting flowfields more complex than the steady flames from which they were derived. Unfortunately, soot scattering signals do not in themselves yield quantitative information about the local soot volume fraction, which is the key soot field parameter tracked in these models. Instead, Rayleigh theory (for small spherical particles: $\pi D/\lambda \ll 1$) predicts that the scattering signal is proportional to the sixth moment of the particle size distribution [16, 17], while fractal agglomerate theory equates the angular scattering intensity to the product of the Rayleigh scattering of the primary particles and a complex moment involving the number of primary particles per agglomerate and the mean agglomerate radius of gyration [18, 19]. Direct measurements of the soot volume fraction are thus more straightforward to interpret than scattering results in making comparisons with soot models and are also important in predicting radiative heat transfer from flames. Here we apply laser extinction and laser-induced incandescence (LII) to determine the soot volume fraction fields in steady and flickering methane/air diffusion flames. Measurements

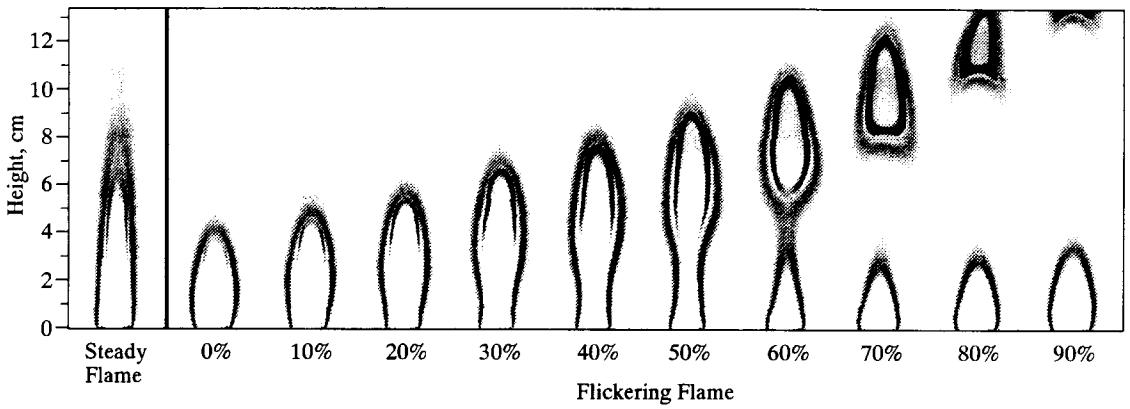

Fig. 1. Laser energy-corrected OH · laser-induced fluorescence and soot scattering images in a steady and time-varying laminar CH_4/air diffusion flame using horizontally polarized light at 283.55 nm. The visible flame height of the steady flame is 79 mm above the fuel tube exit, which is located at the bottom of the images. For the flickering flame, a 0.75-V loudspeaker excitation is employed; ten phase increments separated by 10 ms are shown with an arbitrary zero phase. The OH · fluorescence signals, which surround the intense scattering from the soot particles, have not been corrected for local quenching rates and hence serve as a convenient, qualitative marker of the high-temperature reaction zone. For the full-height images presented here, five single-shot images (32 mm high) have been overlapped. Several of the stacked images have been shifted slightly side-to-side to compensate for flame wobble at higher flame locations.

of soot volume fraction can be combined with single-angle scattering measurements through Rayleigh or Mie theory to estimate mean particle sizes and number densities, providing a phenomenological description of soot production and oxidation processes [17, 20]. Rayleigh theory predicts that only vertically polarized light will be scattered at 90°, and in Mie theory the intensity of horizontally polarized light that is scattered near 90° is highly sensitive to the precise detection angle [21]. Consequently, laser energy-corrected imaging measurements of soot scattering in the steady and flickering flames were made using vertically polarized incident light, supplementing our previous results using horizontally polarized light [1].

EXPERIMENTAL METHODS

Figure 2 shows a schematic diagram of the burner and phase-locked imaging setup, which have been described in detail previously [1]. A coannular axisymmetric burner with a 1.1-cm-diameter fuel tube surrounded by a 10.2-cm air annulus supports an unconfined laminar flame. The mean methane cold flow velocity and air coflow are 7.9 cm/s for both the steady and forced flames. The steady flame has a visible height of 79 mm. A loudspeaker attached to the burner fuel plenum locks the frequency of the flickering flame to the 10.13-Hz repetition rate of the Nd^{3+}:YAG pumped dye laser system. The time delay of the imposed sine wave relative to the laser pulse is controlled with a variable-delay pulse generator, allowing the time-dependent response of the flame to be reproducibly monitored at any given phase. The amplitude of the imposed sine wave is variable. All flickering flame measurements presented here were made with 0.75 V peak-to-peak sine wave forcing, which is an intermediate excitation amplitude of those studied earlier [1].

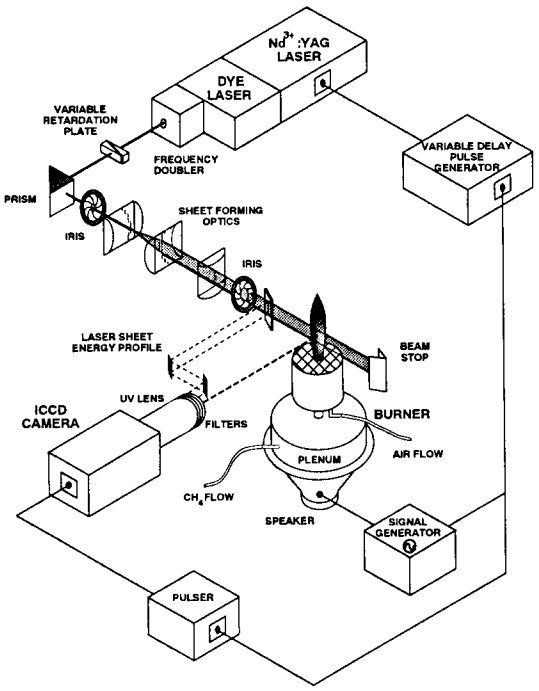

Fig. 2. Experimental set-up for one- or two-dimensional imaging of axisymmetric diffusion flames which are acoustically excited and phase-locked to the pulsed dye laser system operating at 10.13 Hz. For the laser-induced incandescence experiment, the frequency doubler and sheet-forming optics are removed, and a 300 mm focal length lens is used to focus the beam at the center of the flame. Images are recorded using an intensified charge-coupled device (ICCD) camera.

Laser Extinction

Laser light extinction has traditionally been used to measure soot volume fraction. However, both absorption from large molecules, such as polycyclic aromatic hydrocarbons (PAHs), and soot scattering contribute to the extinction signal in addition to soot absorption (the quantity of interest). For the methane/air flames studied here, soot scattering should represent a minor portion of the extinction, since the primary soot particles are small [22] and the extent of soot agglomeration is expected to be limited. However, the contribution of molecular absorption to the measured extinction is of concern, particularly at low soot loadings. Consequently, extinction measurements were performed using the longest wavelength cw laser readily available in our laboratory (632.8 nm—HeNe). In most cases extinction using a shorter wavelength laser source (454.5 nm—Ar^+), where molecular absorption is expected to be much stronger [23], was also measured for comparison with the HeNe results.

In order to perform accurate extinction measurements in these lightly sooting flames

(maximum extinction in the steady flame is ~ 1.5% at 632.8 nm), a laser power stabilizer was used to reduce the noise in the input laser beams to ~ 0.1%, allowing measurement of extinction levels as low as 0.01% after averaging. The Ar^+ laser power was stabilized at 5.0 mW, and the HeNe power was maintained at 1.2 mW. Laser-line notch filters shielded the output port of the stabilizer from luminosity feedback. Small beam movements from thermal lensing on the detector photodiode were an important error source unless minimized through 1-to-1 imaging of the flame centerline, using a lens between the flame and diode [24]. The line-of-sight nature of extinction necessitates data collection along multiple chords and subsequent tomographic inversion to yield locally resolved values of extinction and hence soot volume fraction. To obtain acceptable signal-to-noise, 200 consecutive time records of the amplified photodiode output were averaged using a digital oscilloscope for 0.25 mm spaced radial chords across the width of the flame. Extinction records were tomographically inverted with the 3-point Abel method implemented by Dasch [25]. For the flickering flame, phase-specific extinction profiles were created from the extinction time records using a Pascal-encoded version of Dasch's routine [26].

Laser-Induced Incandescence

Laser-induced incandescence has recently been developed as an alternative method for both relative [27, 28] and quantitative [29] measurement of soot volume fraction. This technique can be configured to avoid the problems of competing signals typical of extinction measurements and can provide instantaneous (i.e., single laser shot) line images or even two-dimensional planar images with an appropriate high-power laser source and detector array. However, the functional dependence of signal variation on particle size is not well understood for practical detection schemes, so the validation and calibration of LII as a measure of soot volume fraction is based on comparison with profiles of soot volume fraction obtained from reliable extinction measurements (e.g., in certain regions of well-characterized steady flames [29]). Here LII was employed as a second means of quantifying the soot volume fraction in both steady and flickering methane/air flames, in order to address concerns over the contribution of molecular absorption to the measured extinction as well as to avoid noise difficulties in the extinction signal which arose at higher positions in the flickering flame (see below).

To perform LII measurements of the soot field, a 300-mm focal length biconvex lens focused the 560-nm output beam from a dye laser at the center of the flame. Computational studies [28, 30] and experimental measurements [28, 29, 31] suggest that once the temperature of the irradiated soot particles reaches the vaporization point (3915 K for graphite [32]) the LII signal remains relatively constant with increasing laser energy. In the present study this signal plateau region occurred for an approximate fluence (spatially and temporally averaged) of 3×10^7 W/cm^2 in both methane and ethylene flames. This value is similar to the critical fluence reported by Tait and Greenhalgh [28] and Quay et al. [29]. In order to minimize signal variations with shot-to-shot laser energy fluctuations, LII measurements were performed at a higher fluence, approximately 7×10^8W/cm^2. Single-shot, one-dimensional line images were recorded on the ICCD camera, with a glass filter providing a detection bandwidth of 300–480 nm. To improve the signal-to-noise in the single-shot data, 10 consecutive frames were collected at each height and averaged after verifying that the peak signal levels were consistent from frame to frame. Higher in the flickering flame the consecutive images often displayed the side-to-side flame wobble which also plagued the time-averaged extinction measurements (see below). In these instances the LII frames were aligned radially and significantly outlying profiles were discarded (typically 2–3 out of 10 at heights above 60 mm) before averaging.

Flame luminosity was approximately ten times weaker than the LII signals in the methane flames and was accounted for by taking a duplicate set of line images with no laser light and subtracting these from the LII line images. An ICCD collection gate of 100 ns was used to maximize the ratio of LII signal to luminosity background (LII signals extend for more than

500 ns after the laser pulse at some flame locations). Broadband laser-induced fluorescence signals can also interfere with LII signals [30] but were negligible in the present experiments.

Soot Scattering

Scattering measurements were made with the same experimental setup and data collection procedure used for the earlier OH · and soot imaging [1]. Dye laser light at 567 nm was frequency doubled to 283.50 nm, and a variable retardation plate (Babinet-Soleil compensator) rotated the incident beam to a vertical polarization relative to the detection axis. Shot-to-shot spatial profiles of the laser energy were recorded via on-camera imaging of a reflection from the incident laser sheet (see Fig. 2). Line profiles of laser energy-corrected scattering at a given height were extracted from the full-height reconstructed images.

RESULTS

Extinction data were obtained at 10-mm increments (from $H = 20$–70 mm above the fuel tube exit) in the steady methane flame and at 20-mm intervals ($H = 20$–160 mm) in the flickering flame. The soot volume fraction was calculated from the tomographically inverted extinction measurements using the Lambert-Beer transmissivity law and the Mie extinction formula in the Rayleigh limit [16, 17, 21]. An index of refraction $\tilde{m} = 1.57 - 0.56i$ was used for both HeNe and Ar^+ wavelengths in order to make direct comparisons with the results of Santoro and coworkers [17, 33]. Figure 3 shows the steady flame HeNe results, which give a maximum soot volume fraction of 3.2 (± 0.3) $\times 10^{-7}$ at $H = 60$ mm. Above $H = 30$ mm in the steady flame, peak soot volume fractions determined from the Ar^+ measurements agree with the HeNe results within $\sim$ 5%–10%, which is within the 15% uncertainty estimated for these measurements. Lower in the flame and along the inner edge of the soot profile, Ar^+ extinction yields larger soot volume fractions, consistent with the expectation of greater absorption by PAH in these regions [17, 34, 35].

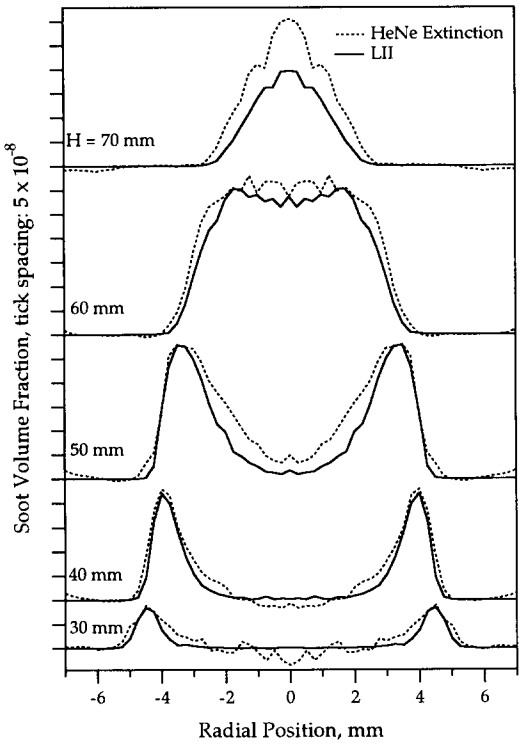

Fig. 3. Soot volume fraction obtained from symmetrized (i.e., averaged about the centerline) HeNe laser extinction (632.8 nm) and laser-induced incandescence (LII) signals at a series of heights in the steady CH_4/air diffusion flame. The zero level has been offset at each height. LII signals have been calibrated by matching the peak signal to the extinction-derived maximum soot volume fraction at $H = 50$ mm.

Figure 3 also includes the comparison of LII signals with the extinction-determined soot volume fractions in the steady methane flame. The peak soot volume fraction at $H = 50$ mm was used to calibrate the LII signal, since at this height and radial location one expects the smallest relative contribution of molecular absorption to the observed extinction [34]. The similarity in location and magnitude of the peak extinction and LII values at different heights indicates that the LII signal indeed closely follows the soot volume fraction. Differences in the two signals towards the center of the profiles may be due to significant molecular absorption at 632.8 nm at these locations, as well as the increased error in the tomographic inversion procedure towards the flame centerline [25].

In Fig. 4 the tomographically inverted, time-resolved extinction data for the flickering flame

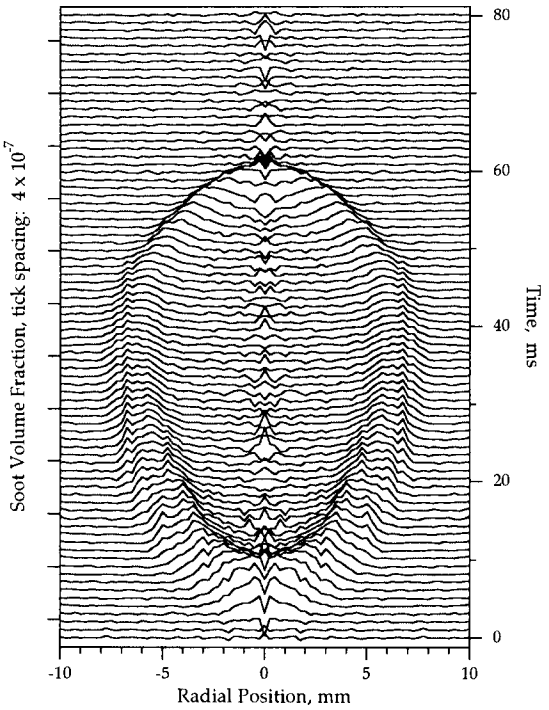

Fig. 4. Time evolution of the soot volume fraction field at $H = 40$ mm in the flickering CH_4/air diffusion flame as derived from HeNe extinction time records. Each line shown is separated by 1 ms in time and staggered by 6×10^{-8} in soot volume fraction. Time progresses from the bottom to the top of the figure, showing first the arrival of soot, the widening of the soot profile into an annular structure as time increases, and finally the convergence of the soot profile to the centerline and its disappearance as the bottom of the clipped-off portion of the flame passes above this measurement height.

are shown for $H = 40$ mm. The soot volume fraction fields higher in the flame are qualitatively similar, with a decreasing time duration of measurable extinction and greater "rippling" noise in the annular soot layer. This noise arises from side-to-side flame wobble during the averaging of the extinction signal over multiple flicker periods. The largest *instantaneous* soot volume fraction (f_v) is $1.3\ (\pm 0.3) \times 10^{-6}$, observed at $H = 120$ mm; this value is four times greater than the maximum f_v in the corresponding steady flame. Another measure of the enhanced soot production can be obtained by area-integrating and time-averaging the extinction profiles over all phases at each height (Fig. 4), then integrating over all heights. This analysis yields an *overall* soot production that is four times larger in the flickering flame compared to its steady counterpart.

LII signals were measured every 10 mm in the flickering flame up to $H = 110$ mm for the ten phase angles shown in Fig. 1. The maximum signal gives a soot volume fraction of $1.5\ (\pm 0.2) \times 10^{-6}$ at $H = 110$ mm (80% phase). Figure 5 shows these results compared with the extinction-derived soot volume fraction for 50% phase. At this instant in time the LII profiles first widen and then contract with increasing height as the soot volume fraction rapidly increases and is subsequently oxidized at the top of the flame. The extinction-derived profiles are generally wider and shorter than their LII counterparts, consistent with the observed flame wobble and the time-averaged nature of the extinction measurement at each radial chord. Difficulties with the tomographic inversion procedure near the centerline are also evident in Figs. 4 and 5.

For vertically polarized incident light the maximum local soot scattering intensity in this flickering flame is ~ 8 times greater than that measured in the corresponding steady flame and occurs in the annular soot region of the clipped-off flame for a phase of 80%. At the same location the enhancement in peak scattering of horizontally polarized light is approximately a factor of 20. Flame tip burnout is complete at about 17 cm in the flickering flame, so it is possible that even greater soot scattering intensities would be found at heights above the current limit for imaging of 13.4 cm.

Uncertainties quoted are one standard deviation, derived from signal variations in repeat measurements of scattering and LII; random errors in the extinction measurements are estimated from noise in the profiles. Calibration of LII in the steady flame may lead to small systematic errors for the time-varying flame results, due to changes in soot particle morphology. Long time-scale movements of the flames remain as a possible source of unquantified error.

DISCUSSION

Changes in residence times, temperatures, and/or local stoichiometries most likely cause the dramatic increase in soot production ob-

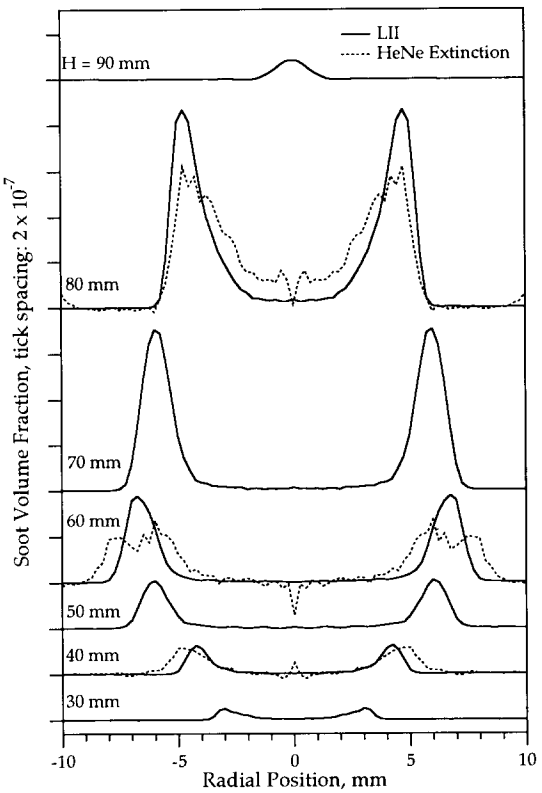

Fig. 5. Laser-induced incandescence signals, interpreted as soot volume fraction, at a series of heights in the flickering CH_4/air diffusion flame at 50% phase. The zero level has been offset at each height. Time-resolved, tomographically inverted HeNe extinction data are also shown at heights of 40, 60, and 80 mm above the burner.

served when a steady CH_4/air flame is induced to flicker. Experimental measurements of the velocity and temperature fields can furnish the data needed to determine differences in time–temperature histories. However, detailed local stoichiometries will be more difficult to characterize and may play a significant role at the base of the clipped portion of the flickering flame, where considerable entrainment and mixing occur. Recent modeling efforts on soot production in time-varying flames [36] should help to identify the key parameters. Estimates of the mean particle sizes and number densities constitute a useful first step in elucidating why soot production is enhanced in the flickering flames. Since fractal agglomerate analysis of soot scattering and extinction data explicitly attempts to account for in-flame soot morphology [37–39], it is intuitively superior to either Rayleigh or Mie analysis, particularly for the calculation of the soot particle number density and surface area. However, application of this approach requires multi-angle scattering data at each spatial location (and phase, in a time-varying flame), which are not available in the present study. Therefore, Rayleigh and Mie analyses have been conducted on our scattering and soot volume fraction data.

Application of Rayleigh or Mie theory requires quantitative, vertically polarized scattering data at a given angle (Q_{vv}), in addition to measurements of soot volume fraction or extinction. In our experiments all scattered light from a vertically polarized incident beam ($Q_{\mathrm{all},v}$) was measured at 90° to the beam propagation direction. Only a small contribution of Q_{hv} to $Q_{\mathrm{all},v}$ is expected, based on the depolarization ratios (Q_{hv}/Q_{vv}) measured at 90° in laminar diffusion flames of methane [40] and ethylene [17, 41]. To quantify our measured scattering intensities, the peak signal at $H = 50$ mm in the steady methane/air flame was matched to the calibrated data of Richardson and Santoro [33] for the same flame conditions. With this single match point the remainder of the steady flame scattering data agree reasonably well. In order to account for the wavelength differences in the two data sets (283.5 vs. 514.5 nm), the calibration scaling factor was multiplied by the wavelength ratio to the fourth power, in keeping with Rayleigh theory [16, 17]. The calibrated LII signals were used as a measure of soot volume fraction, due to their superior signal-to-noise compared to the extinction data (Figs. 3 and 5). Rayleigh and Mie theory calculations were performed using a FORTRAN code with the BHMIE subroutine [42].

Table 1 presents only a small subset of the calculated results: the soot volume fraction, particle diameter, and number densities are given at the point of maximum soot scattering for each measurement height in the steady flame and in the flickering flame at 50% phase. In lieu of velocity measurements, the contour of maximum scattering is used as a rough guide to the time history of soot particles in the steady flame. From the results of Santoro and coworkers [20] for laminar ethylene/air flames, it is clear that the path through the

TABLE 1

Mie Analysis of the Soot Field Along the Contour of Maximum Scattering

Height Above Burner (mm)	Steady Flame			Flickering Flame (50% phase)		
	f_v (10^{-7})	D (nm)	N (10^9 cm^{-3})	f_v (10^{-7})	D (nm)	N (10^9 cm^{-3})
30	0.7 (0.2[a])	39 (5[b])	2.4 (1.3)	0.4 (0.1)	34 (4)	2.0 (1.4)
40	2.2 (0.4)	57 (6)	2.2 (1.1)	1.0 (0.2)	50 (6)	1.5 (0.9)
50	2.3 (0.3)	62 (6)	1.9 (0.8)	2.1 (0.2)	53 (5)	2.7 (1.0)
60	2.2 (0.4)	49 (5)	3.5 (1.8)	3.6 (0.3)	68 (5)	2.2 (0.7)
70	2.0 (0.5)	50 (7)	3.1 (2.2)	6.4 (0.5)	80 (6)	2.4 (0.7)
80				8.1 (0.5)	86 (6)	2.5 (0.7)
90				0.8 (0.2)	85 (11)	0.3 (0.2)

[a] One standard deviation uncertainty estimates.

[b] Diameter and number density uncertainties are the result of propagating volume fraction and scattering error estimates through Rayleigh analysis. These uncertainties agree well with the variation in Mie results over the range of uncertainty in f_v and Q_{vv}.

peak soot volume fraction at all but the lowest heights follows a streamline until the annular character of the soot field disappears due to oxidation. Our results also show that the radial locations of maximum scattering and soot volume fraction generally coincide as long as the annular structure of the soot volume fraction field persists. At higher positions the scattering retains its annular structure longer than the soot volume fraction; however, both the maximum scattering and f_v signals shift to interior streamlines in the steady flame.

Number densities were calculated assuming a monodisperse size distribution at each measurement location. An index of refraction $\tilde{m} = 1.57 - 0.56i$ was used both to calibrate the LII signals to the HeNe extinction results in the steady flame and for the Mie analysis of the scattering at 283.5 nm. Calculations with other literature values for the index of refraction of soot show the same trends evident here. The Rayleigh and Mie results are very similar for particle diameters up to about 60 nm. Mie theory results are presented in Table 1, since there is evidence that for sizes larger than 60 nm they are superior to a Rayleigh description for both the mean volume equivalent diameters and particle number densities when compared with the more accurate fractal agglomerate analysis [38].

In the steady CH_4/air flame the Mie diameters increase up to $H = 50$ mm, and the calculated number densities decrease slightly as soot particle mass growth occurs, possibly reflecting the effects of soot particle agglomeration. From $H = 50$ mm to $H = 70$ mm particle sizes drop from ~ 60 to 50 nm and number densities actually show an increase. The larger number densities present at these heights may result from soot particle inception towards the centerline of the flame, or may also arise from the failure of the monodisperse Mie analysis to account for the high degree of polydispersion in the particle field anticipated at these locations (due to primary particle or agglomerate breakup during oxidation).

At 50% phase in the flickering flame the derived soot particle diameter increases monotonically with height, while the number densities remain roughly constant until oxidation occurs at the top of the flame. In interpreting these results, however, recall that any given phase is a snap-shot in the time-history of the flickering flame. Consequently, soot field properties as a function of height do not imply a temporal record of the soot field, as is the case for steady flames, when traced along a streamline [20]. The Mie results shown in Table 1, when combined with similar trends for all but the greatest heights of the flickering flame, show that particle number densities remain near $2\text{–}3 \times 10^9/\text{cm}^3$ through both the steady and flickering flames, whereas the effective particle diameters increase from a maximum of ~ 60 nm in the steady flame to ~ 90 nm in the flickering flame (using $\tilde{m} = 1.57 - 0.56i$).

However, the extent of particle size increase shown here should not be over interpreted, since the particle size parameters ($x = \pi D/\lambda$) for UV scattering deduced from the Mie results in the flickering flame are large (~ 1) and the deviation between agglomerate and Rayleigh or Mie analysis increases with increasing size parameter [38, 43]. The results of our analysis also do not answer the important question of whether the larger particle sizes apparent in the flickering flames result principally from primary particle growth or increased extent of agglomeration.

CONCLUSIONS

Quantitative soot volume fraction profiles have been obtained for the first time in a flickering hydrocarbon diffusion flame, using tomographic reconstruction of extinction data obtained at 632.8 nm and calibrated laser-induced incandescence measurements. Both measurements show that the instantaneous, peak soot volume fraction in a flickering CH_4/air flame (with 0.75 V loudspeaker excitation) increases by a factor of 4–5 over that in its steady counterpart. The time-averaged, volume-integrated soot volume fraction also shows a four-fold increase. A Mie analysis of the soot field suggests that significantly larger particles are formed in the time-varying flowfield.

We thank Chris Cromer for lending us the laser power stabilizer and George Mulholland and Robert Santoro for insightful discussion of soot formation processes and diagnostic techniques, particularly with regard to the calibration of LII signals.

REFERENCES

1. Smyth, K. C., Harrington, J. E., Johnsson, E. L., and Pitts, W. M., *Combust. Flame* 95:229–239 (1993).
2. Hamins, A., Yang, J. C., and Kashiwagi, T., *Twenty-Fourth Symposium (International) on Combustion*, The Combustion Institute, Pittsburgh, 1992, pp. 1695–1702.
3. Cetegen, B. M., and Ahmed, T. A., *Combust. Flame* 93:15–184 (1993).
4. Chen, L.-D., Seaba, J. P., Roquemore, W. M., and Goss, L. P., *Twenty-Second Symposium (International) on Combustion*, The Combustion Institute, Pittsburgh, 1988, pp. 677–684.
5. Davis, R. W., Moore, E. F., Roquemore, W. M., Chen, L.-D., Vilimpoc, V., and Goss, L. P., *Combust. Flame* 83:263–270 (1991).
6. Ellzey, J. L., and Oran, E. S., *Twenty-First Symposium (International) on Combustion*, The Combustion Institute, Pittsburgh, 1990, pp. 1635–1640.
7. Buckmaster, J., and Peters, N., *Twenty-Third Symposium (International) on Combustion*, The Combustion Institute, Pittsburgh, 1986, pp. 1829–1836.
8. Strawa, A. W., and Cantwell, B. J., *Phys. Fluids* 28: 2317–2320 (1985).
9. Lewis, G. S., Cantwell, B. J., Vandsburger, U., and Bowman, C. T., *Twenty-Second Symposium (International) on Combustion*, The Combustion Institute, Pittsburgh, 1988, pp. 515–522.
10. Pearson, I. G., and Proctor, D., in *Experimental Heat Transfer, Fluid Mechanics, and Thermodynamics 1991* (J. F. Keffer, R. K. Shah, and E. N. Ganic, Eds.), Elsevier, Amsterdam, 1991, pp. 316–322.
11. Vandsburger, U., Seitzman, J. M., and Hanson, R. K., *Combust. Sci. Technol.* 59:455–461 (1988).
12. Syed, K. J., Stewart, C. D., and Moss, J. B., *Twenty-Third Symposium (International) on Combustion*, The Combustion Institute, Pittsburgh, 1990, pp. 1533–1541.
13. Villasenor, R., and Kennedy, I. M., *Twenty-Fourth Symposium (International) on Combustion*, The Combustion Institute, Pittsburgh, 1992, pp. 1023–1030.
14. Leung, K. M., Lindstedt, R. P., and Jones, W. P., *Combust. Flame* 87:289–305 (1991).
15. Honnery, D. R., and Kent, J. H., *Twenty-Fourth Symposium (International) on Combustion*, The Combustion Institute, Pittsburgh, 1992, pp. 1041–1047.
16 Kerker, M., *The Scattering of Light*, Academic, New York, 1969, pp. 31–39.
17. Santoro, R. J., Semerjian, H. G., and Dobbins, R. A., *Combust. Flame* 51:203–218 (1983).
18. Köylü, Ü. Ö., and Faeth, G. M., *Combust. Flame* 89:140–156 (1992).
19. Dobbins, R. A., and Megaridis, C. M., *Appl. Opt.* 30:4747–4754 (1991).
20. Santoro, R. J., Yeh, T. T., Horvath, J. J., and Semerjian, H. G., *Combust. Sci. Technol.* 53:89–115 (1987).
21. D'Alessio, A., in *Particulate Carbon: Formation During Combustion* (D. C. Siegla and G. W. Smith, Eds.), Plenum, New York, 1981, pp. 207–259.
22. Puri, R., Santoro, R. J., and Smyth, K. C., *Combust. Flame* 97:125–144 (1994).
23. Miller, J. H., Mallard, W. G., and Smyth, K. C., *Combust. Flame* 47:205–214 (1982).
24. Montgomery, G. P., and Reuss, D. L. Jr., *Appl. Opt.* 21:1373–1380 (1982).
25. Dasch, C. J., *Appl. Opt.* 31:1146–1152 (1992).
26. Miller, J. H., private communication, 1993.
27. Dec, J. E., zur Loye, A. O., and Siebers, D. L., *SAE Technical Papers Series* SAE-910224, Society of Automotive Engineers, 1991.
28. Tait, N. P., and Greenhalgh, D. A., in *Optical Methods and Data Processing in Heat Transfer and Fluid Flow*, IMechE, London, 1992, pp. 185–193, and *Ber. Bunsenges. Phys. Chem.* 97:1619–1625 (1993).

29. Quay, B., Lee, T.-W., Ni, T., and Santoro, R. J., *Combust. Flame* 97:384–392 (1994).
30. Melton, L. A., *Appl. Opt.* 23:2201–2208 (1984).
31. Eckbreth, A. C., *J. Appl. Phys.* 48:4473–4479 (1977).
32. Leider, H. R., Krikorian, O. H., and Young, D. A., *Carbon* 11:555–563 (1973).
33. Richardson, T. F., and Santoro, R. J., private communication, 1993.
34. Prado, G., Garo, A., Ko, A., and Sarofim, A., *Twentieth Symposium (International) on Combustion*, The Combustion Institute, Pittsburgh, 1984, pp. 989-996.
35. Smyth, K. C., Miller, J. H., Dorfman, R. C., Mallard, W. G., and Santoro, R. J., *Combust. Flame* 62:157–181 (1985).
36 Kaplan, C. R., Baek, S. W., Oran, E. S., and Ellzey, J. L., *Combust. Flame* 96:1–21 (1994).
37. Dobbins, R. A., Santoro, R. J., and Semerjian, H. G., *Twenty-Third Symposium (International) on Combustion*, The Combustion Institute, Pittsburgh, 1990, pp. 1525–1532.
38. Charalampopoulos, T. T., and Chang, H., *Combust. Flame* 87:89–99 (1991).
39. Puri, R., Richardson, T. F., Santoro, R. J., and Dobbins, R. A., *Combust. Flame* 92:320–333 (1993).
40. Garo, A., Lahaye, J., and Prado, G., *Twenty-First Symposium (International) on Combustion*, The Combustion Institute, Pittsburgh, 1986, pp. 1023–1031.
41. Köylü, Ü. Ö., and Faeth, G. M., *J. Heat Transf.* 116:152–159 (1994).
42. Bohren, C. F., and Huffman, D. R., *Absorption and Scattering of Light by Small Particles*, Wiley, New York, 1983, pp. 477–482.
43. Mountain, R. D., and Mulholland, G. W., *Langmuir* 4:1321-1326 (1988).

Received 1 December 1993; revised 20 April 1994